Development of a Framework for Static Aeroelastic Analysis of Flexible Wings including Viscous Flow Effects

David Pina Brandão
david-brandao@tecnico.ulisboa.pt

Instituto Superior Técnico, Lisboa, Portugal

December 2015

Abstract

As the aviation industry demands more efficient aircraft designs, the interaction between structural and aerodynamic behaviors is nowadays of great importance. Especially in novel designs there is an increased interest in accurately predicting the aeroelastic characteristics of such aircraft still in the early stages of development. Employing high fidelity models, such as coupled CFD and CSD approaches, is still today computationally expensive. Low fidelity models, with fast turnaround times, frequently dismiss viscous flow effects. In this work, an expedite procedure for the evaluation of the static aeroelastic characteristics of flexible wings in subsonic flight with inclusion of viscous flow effects is implemented. The aerodynamic loads are evaluated through a Viscous-Inviscid Interaction procedure using an open-source 3D Panel Code coupled with a 2D Boundary Layer solver. Surface velocity is obtained for the inviscid problem, which is then used as boundary condition for solving a set of equations derived from the Von Karman momentum integral along surface sections. Boundary Layer thickness is then taken into account in a new computation of the inviscid flow. After the aerodynamic solution converges, the surface loads are used as input for static structural analysis. The iterative procedure is carried on by updating the displaced geometry for new aerodynamic analysis. This simplified aerodynamic model is therefore able to account for viscous flow effects, namely friction drag and displacement effects. The effect of viscous flow on aeroelastic behavior is assessed and aerodynamic results are compared with commercially available software. The advantages of the method here implemented are then discussed.

Keywords: Aeroelasticity, Viscous-Inviscid Interaction, Integral Boundary Layer, Panel Method

1. Introduction

1.1. Motivation

Aeroleastic effects have a critical influence on aircraft design due to the growing focus on fuel efficiency. Novel greener designs ranging from High Aspect Ratio wings to Joined Wing configurations with better aerodynamic performance also show highly complex static and dynamic aeroelastic coupling. These designs, now possible through the employment of advanced structural solutions such as the use of composite materials and high strength alloys, also have the downside of resulting in structures with greater flexibility, which magnifies the influence of such effects and the importance of including Aerostructural considerations right from the first design stages [12].

Correctly predicting such effects and introducing design solutions right from the first stages of development of a new aircraft can therefore bring multiple advantages. The field of Computational Aeroelasticity (CAE) studies how aeroelastic behavior can be modeled employing models ranging from very simple and expedite models presenting low fidelity results to highly complex but computationally heavy models able to deal with a larger range of flight conditions and phenomena. Although the choice of high fidelity models seems obvious as computational power availability increases, the use of such models in MDO approaches is still very limited by the computational times required to obtain an high-fidelity aerodynamic and aeroelastic solution.

Several authors and commercial packages present aeroelastic solutions across various levels of fidelity. However, the effects of Viscous Flows are usually only taken into account in high-fidelity approaches. This work attempts to fill that gap by including the effects of the presence of a boundary layer on a low fidelity aerodynamic inviscid model.

1.2. Objectives

The main objective proposed for this work is to implement a static aeroelastic analysis framework based in a low-fidelity expedite aerodynamic model

and include viscous flow effects through the implementation of a Boundary Layer model.

Taking into account a study case, the influence of viscous phenomena in static aeroelastic behaviour is also to be discussed through a comparison of the results obtained by including and neglecting such effects.

2. Aeroelasticity

2.1. Problem Formulation

Aeroelasticity is nowadays a well established field, concerned with the study of the interaction between three forces: Aerodynamic, Inertial and Elastic [13]. The three disciplines involved (Fluid Mechanics, Structural Dynamics and Structural Mechanics) were firstly represented together by Collar in the 1940's using a triangle diagram, Figure 1, named after him [2].

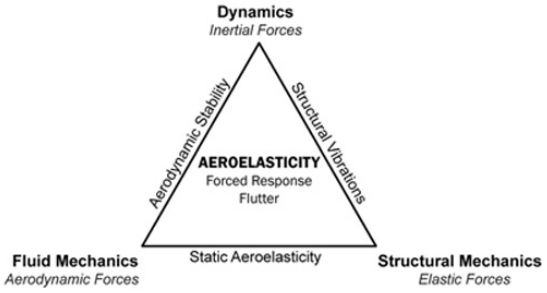

Figure 1: The Collar Diagram, repesenting the three Aeroelastic Forces and their interactions [1].

As a composite of several disciplines, the aeroelastic problem formulation requires inputs from the fields involved. Formally, their interaction can be summarized in the Generalized Equations of Motion 1 and 2 [18].

$$[M]\{\ddot{q}(t)\} + [C]\{\dot{q}(t)\} + [K]\{q(t)\} = \{F(t)\} \quad (1)$$

$$\{w(x,y,z)\} = \sum_{i=1}^{N_{modes}} q_i(t)\{\phi_i(x,y,z)\} \quad (2)$$

In equation 1, on the left side, $q(t)$ represents the generalized displacement vector and $[M]$,$[C]$ and $[K]$ are, respectively, the Mass, Damping and Stiffness matrices. On the right side the generalized force vector $F(t)$ relates the aerodynamic and inertial loads with structural dynamics. In equation 2, $w(x,y,z,t)$ is the structural displacement vector and $\phi_i(t)$ represents the normal modes of the structure [18, 10].

Equation 1 will further simplify for the static conditions as can be seen in equation 3.

$$[K]\{q\} = \{F\} \quad (3)$$

2.2. Computational Aeroelasticity

With the appearance of the fields of Computational Fluid Dynamics (CFD) and Computational Structural Dynamics (CSD), aeroelastic modeling also felt improvements. In fact, these events opened the way for the creation of the field of Computational Aeroelasticity (CAE), which specifically refers to the coupling of different aerodynamic and structural models, varying in capabilities, formulation, approximations, fidelity and computation times, for the study of Fluid/Structure Interaction (FSI) problems [2]. This allows the user to tailor the model and it's approximations to the purposes and conditions of each study.

As previously seen in equation 1, it implies that Aerodynamic Loads computed by the Fluid Dynamics solver must be transfered to the Structural solver. If the computation is stopped at this point a One-Way Coupled model is being employed, meaning that the aerodynamic model is not updated to the deformed configuration. This implies that a considerable error is present in the results as the Aerodynamic and Structural geometries do not coincide.

In order to obtain a properly converged solution, the Structural displacements have to be taken into account to update the Aerodynamic geometry after a deformed configuration is obtained. This kind of model is what is called a Two-Way Coupling procedure (Figure 2). After convergence, the calculated aerodynamic loads match the deformed structure shape.

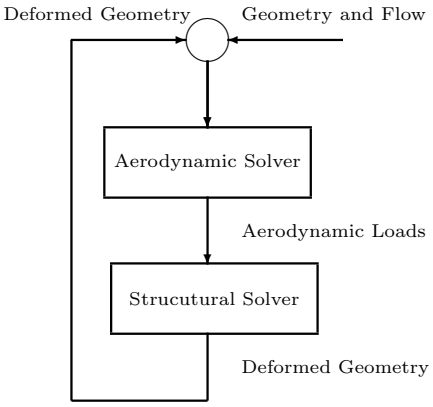

Figure 2: Two-Way Aeroelastic Coupling.

Another question that can be raised regarding the model coupling is related to how independent the solvers and formulations of each discipline are in relation to the other. Kamakoti [10] sorts the models into three categories, according to how tightly connected the solution procedures are.

Fully-Coupled Models occupy the top of this scale. In this kind of approach, the problem's formulation

is developed so that the aerodynamic and structural governing equations are solved together. Although this avoids the iterative procedure between the aerodynamic and structural solutions, the size of the problems is limited to relatively small ones, being only applied in 2D cases.

On the opposite side of the scale appear the *Loosely-Coupled Models*. In this case each solution is obtained in separated solvers and an iterative procedure between the two disciplines is executed until convergence is achieved [17]. The main advantage of using such a method is the possibility to use existent, proven solvers in each of the disciplines. On the other hand, the need of an interface for the data transfer, usually through output and input files, leads to large computation times.

As a compromise between the former methods, the *Closely-Coupled Models* emerge as the most frequently used kind [10]. As in the *Loosely-Coupled Model*, the solution is obtained from an iterative procedure and, while the Aerodynamic and Structural equations are still solved separately, both solvers are implemented into one single package, significantly improving information exchange between solvers [17].

Several load and displacement transfer methods were developed. These can fall into two categories, according to Kennedy [12].

The first one is *Direct transfer*, where aerodynamic loads are directly transfered to the structure model either by interpolating the data in that same geometric surface or using rigid links to transfer the loads and displacements. This was the method implemented by Kennedy et al. [12] and James et al. [9].

A second method can be employed when geometry gaps exist between the models, which consists in evaluating the contribution of the load distribution by integrating it along an intermediate auxiliary surface or the aerodynamic surface itself. The resultant equivalent forces and moments are then transfered to the structure.

In what respects the methods used to model the Aerodynamics of aircraft, Bartels [2] suggests three major fidelity levels can be identified: *Low*, *Moderate* and *High Fidelity*.

Low Fidelity aerodynamic methods used to model lifting bodies include Panel Methods, Doublet and Vortex Lattice Methods (DLM and VLM), Lifting Line and Lifting Surface methods, among others. These compute the inviscid flow quickly as they do not require to discretize the entire fluid volume. The geometry can be easily modeled or imported from CAD models. These linear models are still today frequently used in the industry coupled with FEM structural models, mainly in early design phases and optimization codes due to the quick turnaround times and relatively accurate results.

CFD based approaches, on the other hand, offer better accuracy and are capable of dealing with complex geometries and modeling several kinds of non-linear aerodynamic phenomena, depending on the Aerodynamic models used. These approaches fall inside the *High fidelity* models and solve a version of the non-linear Navier-Stokes equations like the Reynolds-averaged Navier-Stokes (RANS) over the full discretized flow domain coupled with turbulence models. However, such models are computationally expensive and present a more complex discretization process, appropriate modeling relies significantly on the user expertise.

Moderate Fidelity models are usually a simplified or linearized version of the Navier-Stokes or Euler equations solved in the entire flow domain. Reducing computational costs up to an order of magnitude when compared with the nonlinear counterpart, this method was considered sufficient in many cases [10].

Another kind of models that can be considered to present Moderate Fidelity are the ones based in Viscous-Inviscid Interaction (VII) procedures which couple inviscid and viscous approximations to the flow field equations to get the final solution. Commercially available software packages like *ZEUS* use an Euler equation solver for the inviscid part of the flow coupled with a steady boundary-layer equation to include viscous effects. The use of this kind of models for aeroelastic analysis is however not very frequent. In purely aerodynamic problems this is also the approach followed by several authors. Drela in [4, 5] uses the same approach of coupling an Euler CFD Inviscid code with Integral Boundary Layer solutions along the surface. Regarding VII models based on Panel Methods, one of the earliest codes to implement such model was VSAERO in 1987 [14], where 3D Panel Method was coupled with 2D Boundary Layer Equations solved along streamlines on the surface wing. It was however limited to incompressible flows and small separation regions. In 1997, Milewsky [15] presented a VII procedure using a low-order 3D Panel Method coupled with 3D Boundary Layer equations for application in the naval industry. This more generic formulation of the Boundary Layer presented good results regarding the estimation of Loads and Boundary Layer quantities. More recently, Stalewski et al. [20] implemented an inviscid model solved using a Boundary Element Method coupled with 2D Boundary Layer Equations in the frame of the European Union 6th Framework Program for a light general aviation aircraft. When accounting for viscous flow effects over the fuselage, all these codes either dismissed them or assumed the axisimetry of the flow. Pereira et al. [16] implemented a 3D Panel

Method coupled with a 3D Boundary Layer code capable of dealing with transverse flows, demonstrating a correct prediction the position of longitudinal vortices around the nose of a streamlined train.

3. Aeordynamic models

The method picked for modeling the Inviscid flow is a 3D Panel Method code, APAME. Modifications to allow for the VII procedure to be done are presented. For the Viscous Boundary Layer, integral relations based on the Von Karman momentum integral equation are employed, along with a Lag-Entrainment for upstream history effects method and empirical closure relations for both Laminar and Turbulent flows. These models are described next.

3.1. Panel Methods

The method used in this work is the Constant-Strength Combined Source and Doublet Panel Method, presented in [11]. It was chosen because it represents a good agreement between complexity, generality and computational time, as well as facilitating a posterior Viscous-Inviscid Interaction procedure by the modification of the source strengths.

Taking this into account, a solution for the Laplace equation can be built. The representation of the main definitions needed is done in Figure 3.

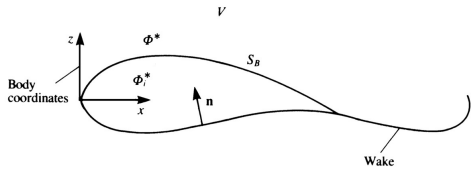

Figure 3: Potential flow over closed body and definitions.[11]

For a distribution of source, σ, and doublet, μ, singularity strengths along surface S_b and the free stream potential $\Phi_\infty = u_\infty x + u_\infty y + u_\infty z$, the total potential Φ^* at any point (x, y, z) in the domain V is given by Equation 4.

$$\begin{aligned}\Phi^*(x,y,z) =& \frac{1}{4\pi}\int_{body+wake} \mu \mathbf{n}\cdot\nabla\left(\frac{1}{r}\right) dS \\ &- \frac{1}{4\pi}\int_{body} \sigma\left(\frac{1}{r}\right) dS \\ &+ \Phi_\infty,\end{aligned} \tag{4}$$

Applying the Dirichlet Boundary Condition by enforcing $\Phi_i^*(x,y,z) = \Phi_\infty$, and dividing the model into N surface panels and N_W wake panels, Equation 5) is obtained.

$$\begin{aligned}&\sum_{k=1}^{N}\frac{1}{4\pi}\int_{\text{body panel}} \mu \mathbf{n}\cdot\nabla\left(\frac{1}{r}\right) dS \\ &+\sum_{j=1}^{N_W}\frac{1}{4\pi}\int_{\text{wake panel}} \mu \mathbf{n}\cdot\nabla\left(\frac{1}{r}\right) dS \\ &-\sum_{k=1}^{N}\frac{1}{4\pi}\int_{\text{body panel}} \sigma\left(\frac{1}{r}\right) dS = 0,\end{aligned} \tag{5}$$

This assumption also sets the source strength values along the wing surface (Equation 6), leaving the only doublet strengths to be discovered.

$$\sigma = \mathbf{n}\cdot\mathbf{Q}_\infty \tag{6}$$

The integral terms in Equation 5 define the influence of one specific singularity distribution disposed along a given panel in any point inside V. By summing the influence of all panels it is possible therefore to determine the potential in any point due to the entire surface and wake. However, as doublet strengths of each panel are still unknown, the boundary condition has to be applied as described at each internal point in order to correctly define the geometry seen by the flow. This is enforced at every *Collocation Point*, positioned at the center of each panel that defines the body surface, slightly deviated towards the inside of the airfoil/wing.

The wake doublet distribution strength is dictated by the Kutta Condition at the Trailing Edge, as expressed in Equation 7,

$$\mu_w = \mu_u - \mu_l, \tag{7}$$

where μ_u and μ_l are respectively the doublet strengths at the last upper and lower panels along the trailing edge.

Employing constant-strength singularity panels, the singularity strengths μ and σ can be taken outside of the integrals in Equation 5 and the remaining integral terms become only dependent on the geometry of the panel and the position of the point being evaluated, giving origin to the Influence Coefficient matrices C_k, C_l and B_k. Equation 8 must then be solved for each Collocation Point.

$$\sum_{k=1}^{N} C_k\mu_k + \sum_{l=1}^{N_W} C_l\mu_l + \sum_{k=1}^{N} B_k\sigma_k = 0 \tag{8}$$

Equation 8 can still be arranged. Defining a new Influence Coefficient matrix A_k,

$$A_k = \begin{cases} C_k & \text{if not Trailing Edge panel} \\ C_k \pm C_t & \text{if Trailing Edge panel} \end{cases}, \tag{9}$$

where C_t is the influence coefficient of the first wake panels, the simplified Equation 10 can be obtained.

$$\sum_{k=1}^{N} A_k \mu_k = -\sum_{k=1}^{N} B_k \sigma_k \tag{10}$$

This equation has to be evaluated at each of the N collocation points, originating a system of N equations with N unknowns that can now be solved. Generalizing for all kinds of panel methods and adapting from the nomenclature used in [6], this system of equations can be represented as

$$[AIC]\{\lambda\} = \{RHS\}, \tag{11}$$

where $[AIC]$ is the Aerodynamic Influence Coefficients matrix, $\{\lambda\}$ is the vector of the unknown singularity strengths and $\{RHS\}$ is the Right-Hand Side containing the known parameters, in this case the influence coefficients multiplied by the source strengths obtained from the boundary conditions.

Influence coefficients are still defined in a generic way. For a 3D body, the velocity potential can be evaluated at an arbitrary point $P = (x, y, z)$, generated by a quadrilateral rectilinear panel with a constant strength source distribution and with a constant strength doublet distribution. The equations used are presented in [11, 7] and are not presented here not to lengthen the discussion.

3.2. Integral Boundary Layer

The Von Karman Equation (Equation 12) appears from the integration of the Thin Shear layer momentum equation.

$$\frac{\xi}{\theta}\frac{d\theta}{d\xi} = \frac{\xi}{\theta}\frac{C_f}{2} - \left(\frac{\delta^*}{\theta} + 2 - M_e^2\right)\frac{\xi}{u_e}\frac{du_e}{d\xi}, \tag{12}$$

where δ^* and θ are the displacement and momentum thicknesses and C_f is the skin friction coefficient.

By introducing a few more integral parameters, density thickness δ^{**}, kinetic energy thickness θ^* and dissipation coefficient C_D, and shape parameters H, H^* and H^{**}, the shape parameter equation (13) can then be obtained by multiplying by u and integrating.

$$\begin{aligned}\frac{\xi}{H^*}\frac{dH^*}{d\xi} =& \frac{\xi}{\theta}\frac{2C_D}{H^*} - \frac{\xi}{\theta}\frac{C_f}{2} \\ &- \left(\frac{2H^{**}}{H^*} + 1 - H\right)\frac{\xi}{u_e}\frac{du_e}{d\xi}\end{aligned} \tag{13}$$

The Von Karman equation (12) can be rewritten as in Equation 14.

$$\frac{\xi}{\theta}\frac{d\theta}{d\xi} = \frac{\xi}{\theta}\frac{C_f}{2} - \left(H + 2 - M_e^2\right)\frac{\xi}{u_e}\frac{du_e}{d\xi}. \tag{14}$$

As the system constituted by Equations 13 and 12 still possesses more than 2 independent variables, closure relations will have to be included, introducing assumptions depending on the kind o flow (Laminar, Turbulent or Transition). By defining δ and θ as dependent variables, the remaining ones, H^*, H^{**}, C_f and C_D, will have to be modeled with such relations.

The kinematic shape parameter, H_k, as is defined in Equations 15.

$$H_k = \frac{H - 0.290M_e^2}{1 + 0.113M_e^2}, \tag{15}$$

For Laminar Flow, taking into account the Falkner-Skan one-parameter profiles, Drela [3] obtains the expressions bellow.

$$H_k^* = \begin{cases} 1.515 + 0.076\frac{(4-H_k)^2}{H_k} & \text{for } H_k < 4 \\ 1.515 + 0.040\frac{(H_k-4)^2}{H_k} & \text{for } H_k > 4 \end{cases} \tag{16a}$$

$$H^* = \frac{H_k^* + 0.028M_e^2}{1 + 0.014M_e^2} \tag{16b}$$

$$Re_\theta \frac{C_f}{2} = \begin{cases} -0.067 + 0.01977\frac{(7.4-H_k)^2}{H_k-1} \\ \qquad\qquad \text{for } H_k < 7.4 \\ -0.067 + 0.022\left(1 - \frac{1.4}{H_k-6}\right)^2 \\ \qquad\qquad \text{for } H_k > 7.4 \end{cases} \tag{17}$$

$$Re_\theta \frac{2C_D}{H^*} = \begin{cases} 0.207 + 0.00205(4 - H_k)^{5.5} \\ \qquad\qquad \text{for } H_k < 4 \\ 0.207 - 0.003\left(H_k - 4\right)^2 \\ \qquad\qquad \text{for } H_k > 4 \end{cases} \tag{18}$$

Also from Whitfield, an expression for the density thickness parameter H^{**} is presented in Equation 19, which will be used for both turbulent and laminar flows.

$$H^{**} = \left(\frac{0.064}{H_k - 0.8} + 0.251\right)M_e^2, \tag{19}$$

As for turbulent flow, a skin friction coefficient relation is applied as presented in [4], specifically in this case the one developed by Swafford and presented in Equation 20.

$$\begin{aligned}F_c C_f =& 0.3e^{-1.33H_k}\left[\log_{10}\left(\frac{Re_\theta}{F_c}\right)\right]^{-1.74-0.31H_k} \\ &+ 0.00011\left[\tanh\left(4 - \frac{H_k}{0.875}\right) - 1\right],\end{aligned} \tag{20}$$

with

$$F_c = (1 + 0.2M_e^2)^{\frac{1}{2}}. \quad (21)$$

Regarding the energy thickness shape parameter H^* in turbulent flow, Drela [4] used Swafford's expression for the velocity profile to derive the closure relation present in Equation 22.

$$H_k^* = \begin{cases} 1.505 + \frac{4}{Re_\theta} + \left(0.165 - \frac{1.6}{\sqrt{Re_\theta}}\right)\frac{(H_0 - H_k)^{1.6}}{H_k} \\ \qquad\qquad \text{for } H_k < H_0 \\ 1.505 + \frac{4}{Re_\theta} + (H_k - H_0)^2 \\ \left[\frac{0.04}{H_k} + 0.007\frac{\log(Re_\theta)}{\left(H_k - H_0 + \frac{4}{\ln(Re_\theta)}\right)^2}\right] \\ \qquad\qquad \text{for } H_k > H_0 \end{cases} \quad (22)$$

with,

$$H_0 = 3 + \frac{400}{Re_\theta}, \quad (23)$$

As for C_D, as developed in [4, 5], the dissipation coefficient comprehends the sum of two contributions, one from a wall layer and another from a wake layer (Equation 24).

$$C_D = \frac{C_f}{2}U_s + C_\tau(1 - U_s), \quad (24)$$

where C_τ represents the magnitude of the shear stresses in the wake, and the normalized wall slip velocity U_s is given by Equation 25.

$$U_s = \frac{H^*}{2}\left(1 - \frac{4}{3}\frac{H_k - 1}{H}\right), \quad (25)$$

C_τ is obtained by solving a rate equation (26) used in [4, 5] which introduces an history effect into the boundary layer.

$$\frac{\delta}{C_\tau}\frac{dC_\tau}{d\xi} = 4.2(C_{\tau EQ}{}^{1/2} - C_\tau^{1/2}), \quad (26)$$

where the nominal boundary-layer thickness δ and the equilibrium shear stress coefficient $C_{\tau EQ}$ are given by:

$$\delta = \theta\left(3.15 + \frac{1.72}{H_k - 1}\right) + \delta^*, \quad (27)$$

$$C_{\tau EQ} = H^*\frac{0.015}{1 - U_s}\frac{(H_k - 1)^3}{H_k^2 H} \quad (28)$$

During the computation of the laminar stages there is still the need to detect the point where transition occurs. To do so, the evaluation of the amplification of small disturbances made using the e^9 *method* [4, 5].This is achieved by solving Equation 29 along with Equations 13 and 14.

$$\frac{d\tilde{n}}{d\xi}(H_k, \theta) = \frac{d\tilde{n}}{dRe_\theta}(H_k)\frac{m(H_k) + 1}{2}l(H_k)\frac{1}{\theta}, \quad (29)$$

where $m(H_k)$ and $l(H_k)$ are the empirical relations,

$$l(H_k) = \frac{6.54H_k - 14.07}{H_k^2}, \quad (30)$$

$$m(H_k) = \left(0.058\frac{(H_k - 4)^2}{H_k - 1} - 0.068\right)\frac{1}{l(H_k)}, \quad (31)$$

At the wake the relations used until here are still valid. The wake is assumed to always be turbulent and the condition of $C_f = 0$ is enforced.

4. Implementation

4.1. 3D Aerodynamic Module

The 3D Panel Method code used for obtaining the inviscid solution of the flow around the 3D wing was APAME, developed by Daniel Filkovic [7]. This code, written in FORTRAN, allows the user to import an already discretized surface model from NASTRAN, ABAQUS or other Structural and CFD commercial solvers output and input files and generating a Panel Model for Static Aerodynamic Analysis.

In order to enable a VII procedure to be done, some modifications had to be implemented to the source code in order to include effects of Boundary Layer displacement. A portion of code to read a file with the Transpiration Velocity was included. These values are then included in the source strength distribution at each panel. The transpiration velocity w can be obtained from the evolution of the inviscid velocity on the edge of the boundary layer, u_e, and the displacement thickness δ^* as shown by Equation 32.

$$w(x, 0) = \frac{d(u_e\delta^*)}{dx}, \quad (32)$$

After the geometry is imported it is then interpreted. A routine implemented in MATLAB assembles the correspondent streamwise sections for the 2D Boundary Layer Solver. After the boundary layer is evaluated for all sections, the results are reassembled and passed to the 3D aerodynamic model. The APAME Solver is once again called to solve the inviscid problem but his time with the displacement correction. This is done iteratively until convergence is achieved.

4.2. Structural Module

The Structural module is responsible for calculating the solution to the static structure problem. Its main component is NX NASTRAN, a commercial Finite Element Analysis tool that solves the structural linear system consisting of the wing structure fixed at the root and loaded with different aerodynamic loads.

The Aerodynamic pressure and the shear stresses are organized and passed to the NASTRAN structural analysis file, replacing any existent load cases.

NX NASTRAN is then called and the results output file is generated containing, among other parameters, the nodal displacements to be included in the aerodynamic model.

4.3. Aeroelastic Framework

The implementation of the Aeroelastic framework around the two main modules is summarized in the flowchart of Figure 4.

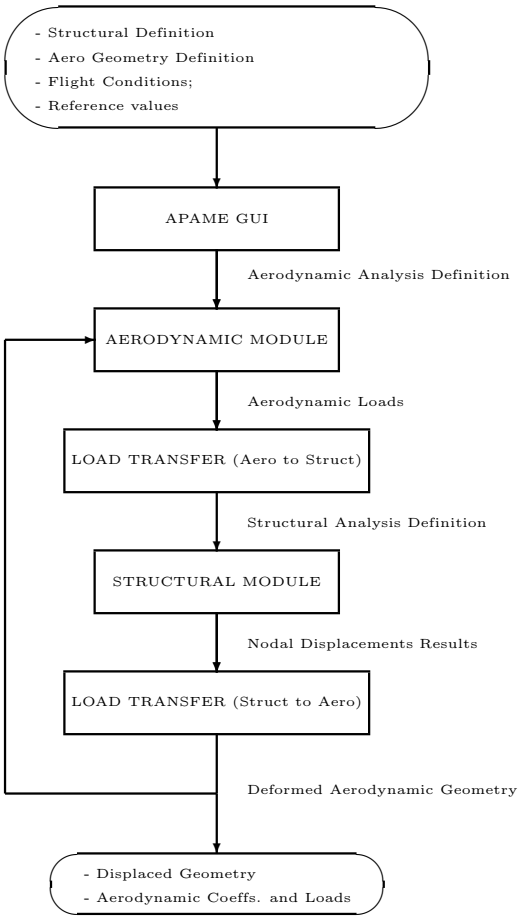

Figure 4: Aeroelastic Framework Modules flowchart.

5. Study Case Definition

The wing geometry to be studied is a reference wing for the NOVEMOR project of the 7th EU Framework, modified in [19] to present an high aspect ratio of 12. It has a wingspan of 36.33 meters and a Mean Aerodynamic chord of 3.02 meters. Figure 5 is a representation of the wing geometry.

Two Test Cases were defined for Mach 0.5, at an altitude of 20000 feet, considering ISA conditions. The first test case corresponds to the trimmed flight condition of this aircraft. For the aircraft Maximum Takeoff Weight of 58000kg the angle of attack for trim condition was calculated to be 6.95. As for the second test case, the same altitude and Mach speed were assumed, changing only the angle of attack to

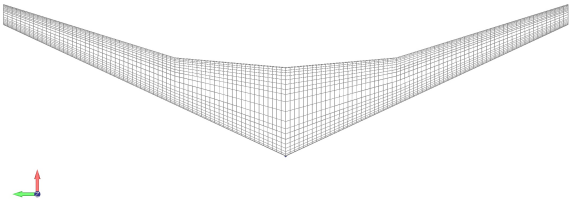

(a) Top view

Figure 5: Three view wing geometry sketch.

3.5.

The structural model was based in conventional wing structure configuration, shown in Figure 6. All elements were modeled as CQUAD4 plate elements.

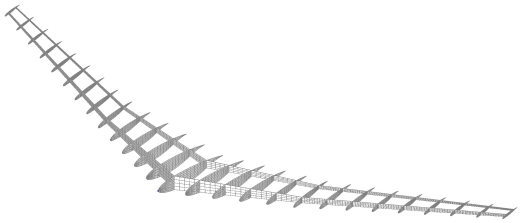

Figure 6: Wing structure Finite Element Model: Spars (longitudinally) and Ribs (transverselly).

6. Aerodynamic Analysis Results

A VII Aerodynamic analysis with the Aerodynamic Module here implemented for Case # 2 is presented. Figure 7 shows the convergence of some aerodynamic coefficients with the iteration number.

Regarding the case where $\alpha = 3.5$, from the 5th iteration the result can be considered converged. From then on, the results always oscillate bellow 1%, as can be seen in Figure 8. For the other test case, where $\alpha = 6.95$, the convergence of results is not as good with the increase of the iteration number, with oscillations around 10%. This may be due to the incapacity of the implemented model to deal with boundary layer separation that may occur at such angles of attack.

The obtained VII solutions were compared to the inviscid solution obtained with APAME and with a solution obtained with a CFD commercial package, StarCCM+. The model employed was a Reynolds Averaged Navier-Stokes (RANS) model with an SST (Menters Shear Stress Transport) $k-\omega$ turbulence model. The comparison of results from the VII code, CFD and APAME are presented in Table 1.

Every aerodynamic coefficient was calculated to an error smaller than 3% by the VII code when

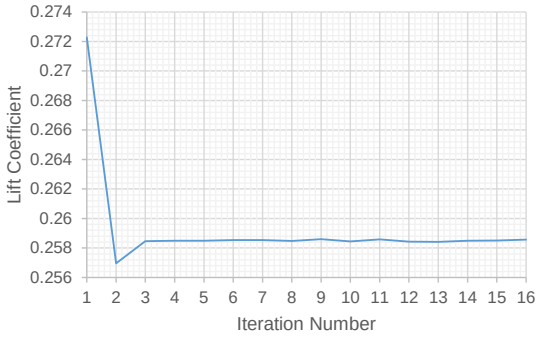

(a) Convergence of the lift coefficient with $\alpha = 3.5$.

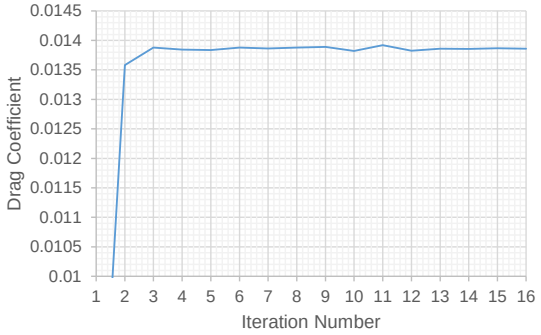

(b) Convergence of the drag coefficient with $\alpha = 3.5$.

Figure 7: Convergence of the aerodynamic results with the iteration number for both test cases.

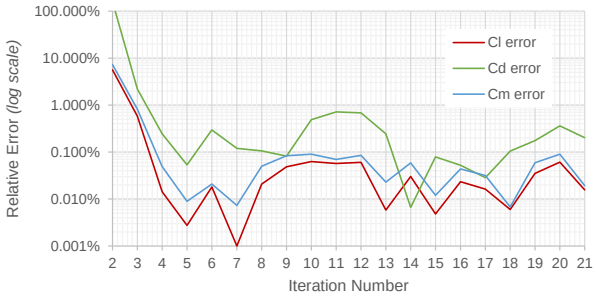

Figure 8: Evolution of the Relative Error of the aerodynamic coefficients with the iteration number for $\alpha = 3.5$.

compared to the CFD solution. The biggest deficiency in the Inviscid solver is the prediction of Drag, which was underestimated with an error of -62.5%, while an error of -0.8% was obtained by the VII code.

The computational effort was almost 50 times lower for the VII code computation than for the CFD analysis (see Table 2).

7. Aeroelastic Analysis Results

The Aeroelastic results are presented in detail for Case #2, starting from the inviscid assumptions. The solution for the maximum displacements in

Table 1: Comparison of aerodynamic coefficient results between StarCCM+ CFD solution, the VII code implemented and APAME inviscid solution.

INV vs. CFD	APAME	StarCCM+	Error
C_L	0.272	0.252	**8.2**%
C_D	0.00524	0.01397	**−62.5**%
C_{m_0}	−0.3387	−0.31019	**9.2**%
VII vs. CFD	**VII code**	**StarCCM+**	**Error**
C_L	0.258	0.252	**2.7**%
C_D	0.01385	0.01397	**−0.8**%
C_{m_0}	−0.31679	−0.31019	**2.1**%

Table 2: Comparison of Nomalized CPU computational times for the solution obtained with StarCCM+, the VII code implemented and APAME inviscid code.

	CPU Time *(hours)*		
	APAME	VII code	StarCCM+
CASE #1	0.022	2.15	114.67
CASE #2	0.022	2.326	112.4

each axis, shown in Figure 9, was obtained and the most prominent deflection occurred in the Z axis, which is not only along the general direction of actuation of the Lift force, but also corresponds to the least stiff direction of the wing structure. Convergence of the displacements takes 10 iterations.

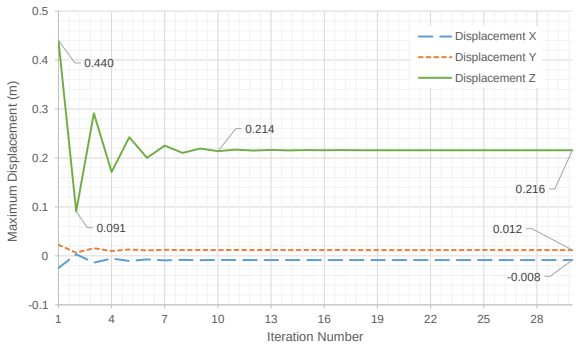

Figure 9: Evolution of x, y and z maximum displacements with iteration number for Inviscid Aerostrucural analysis for Case #2.

In Figure 10 the same parameters are presented for the viscous analysis. The displacements also converge for around 10 aerostructural iterations (Figure 10), with 7 VII iterations each.

Table 3 compares the results obtained for the Viscous and Inviscid analysis. The same tendencies are observed for the Viscous case. However the displacements present a reduced magnitude, for exam-

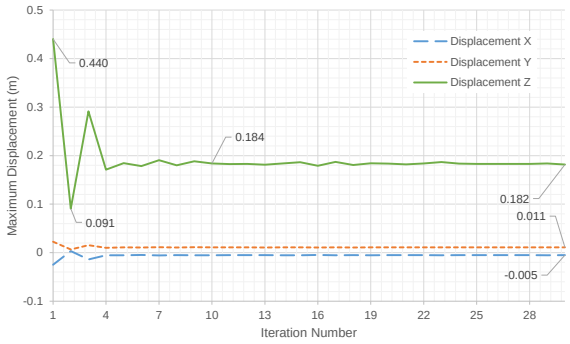

Figure 10: Evolution of x, y and z maximum displacements with iteration number for Viscous Aerostrucural analysis for Case #2.

ple, in the order of 3 cm in the Z direction. This is primarily a result of the reduction of lift due to the presence of the boundary layer. The bigger differences are still in Drag, where a difference of 137% between both models is encountered.

Table 3: Summary of the results obtained for the Aeroelastic analysis of Case #2.

	Inviscid	Viscous	Difference
Max. disp. (m)	0.216	0.182	**-16%**
Max. tors. (deg)	-0.834	-0.746	**-11%**
Cl	0.250	0.237	**-5%**
Cd	0.005	0.013	**137%**
Cm	-0.297	-0.276	**-7%**
CPU time (s)	1.672	10.403	**522%**

In Figure 11 the deformed wing shape for this case is represented.

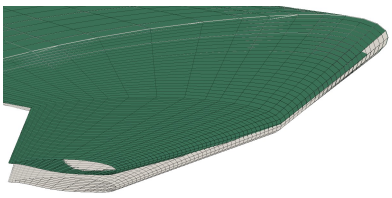

Figure 11: Deformed Wing shape after converged Viscous Aerostructural Solution is obtained for Case #2.

Moving to the Case # 1, the same tendencies are observed. However, the displacements are significantly more prominent due to the higher Lift generated. Table 4 compares the results obtained by the Inviscid and VII codes.

The comparison between both cases and the analysis of the difference between the Inviscid and Viscous results show that Viscous effects are more influent in the final displacements for the low lift conditions. For high lift conditions the importance of inviscid effects rises in comparison to the viscous effects.

Table 4: Summary of the results obtained for the Aeroelastic analysis of Case #1.

	Inviscid	Viscous	Difference
Max. disp. (m)	1.343	1.28354	**-4.43%**
Max. tors.(deg)	-2.56874	-2.38851	**-7.02%**
Cl	0.53809	0.51284	**-4.69%**
Cd	0.0125	0.01907	**52.54%**
Cm	-0.6897	-0.6505	**-5.68%**
CPU time (s)	1.25	10.7988	**763.90%**

Figure 12 shows the deformed geometry for this case.

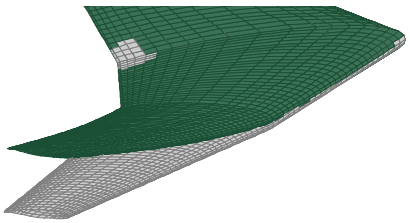

Figure 12: Detail of the deformed wing shape after converged Viscous Aerostructural Solution is obtained for Case #1.

Regarding the computational effort, the inviscid solutions had by far the fastest turnout time. Although the VII computational time is bigger than the inviscid solution, the accuracy is improved. Nevertheless this code is still significantly faster than a CFD based solution, as the cases reported in [8, 17].

8. Conclusions

Good agreement with a commercially available CFD solver, both in the Inviscid and Viscous cases, with the VII code presenting errors of less than 5% in the estimation of aerodynamic coefficients for the higher angle of attack and of less than 3% for the lower angle of attack.

As for the Aerostructural solution, the final test configuration was run, both for the Inviscid and Viscous cases. Convergence occurred at a faster rate for the lower angle of attack case. For the higher angle of attack, the maximum vertical displacement observed was 1.34 meters for the Inviscid computation, which can be compared to the 1.28 meters obtained for the viscous solution. The inclusion of the boundary layer resulted in a reduction of 4.43% in the maximum displacement, which contributed to the 4.69% reduction in Lift. Cd was the parameter that showed a greater difference of more than 50%,

as was already expected from the aerodynamic analysis. For the lower angle of attack the differences in the displacements reached 16% when compared to the inviscid solution. The aerodynamic coefficients also showed bigger differences.

The method here implemented has the advantage of being up to 10 times faster than CFD-based codes, but still accounting for the main viscous effects that affect static aeroelastic phenomena. Although the effect of viscosity is not very perceivable in the maximum displacements, their effect is still considerable, especially if aerodynamic coefficients are to be obtained.

References

[1] Aeroelasticity in turbomachines: Introduction to aeroelasticity. Online, `http://gtt.epfl.ch/page-63561-fr.html`, December 2014. Accessed on October 11th, 2015.

[2] R. E. Bartels and A. I. Sayma. Computational aeroelastic modelling of airframes and turbomachinery: progress and challenges. *Philosophical transactions. Series A, Mathematical, physical, and engineering sciences*, 365(1859):2469–2499, 2007.

[3] M. Drela. A new transformation and integration scheme for the compressible boundary layer equations, and solution behavior at separation. Master's thesis, Massachusetts Institute of Technology, 1983.

[4] M. Drela. *Two-dimensional Transonic Aerodynamic Design and Analysis using the Euler Equations*. PhD thesis, Massachusetts Institute of Technology, 1985.

[5] M. Drela and M. B. Giles. Viscous-inviscid analysis of transonic and low reynolds number airfoils. *AIAA Journal*, 25(10):1347–1385, 1987.

[6] L. L. Erickson. Panel methods: An introduction. NASA Technical Paper 2995, 1990.

[7] D. Filkovic. Graduate work. Master's thesis, Faculty of Mechanical Engineering and Naval Architecture, University of Zagreb, 2008.

[8] D. Huixue, Y. Zhichun, and L. Yi. Accelerated loosely-coupled cfd/csd method for nonlinear static aeroelasticity analysis. *Aerospace Science and Technology*, 14(4):250–258, 2010.

[9] K. A. James, G. J. Kennedy, and J. R. Martins. A review of numerical fluids/structures interface methods for computations using high-fidelity equations. *Computers and Structures*, 134(1):31–41, 2014.

[10] R. Kamakoti and W. Shyy. Fluid-structure interaction for aeroelastic applications. *Progress in Aerospace Sciences*, 40:535–558, 2004.

[11] J. Katz and A. Plotkin. *Low-Speed Aerodynamics*. Cambridge University Press, 2^{nd} edition, 2001. ISBN:978-0-521-66552-0.

[12] G. Kennedy and J. Martins. A parallel aerostructural optimization framework for aircraft design studies. *Structural and Multidisciplinary Optimization*, 2014.

[13] J. G. Marshall. A review of aeroelasticity methods with emphasis on turbomachinery applications. *Journal of Fluids and Structures*, 10:237–267, 1996.

[14] B. Maskew. Program vsaero: A computer program for calculating the non-linear aerodynamic characteristics of arbitrary configurations. User's manual, NASA, 1982.

[15] W. M. Milewski. *Three-dimensional viscous flow computations using the integral boundary layer equations simultaneously coupled with a low order panel method*. PhD thesis, Massachusetts Institute of Technology, June 1997.

[16] I. Pereira and J. M. C. S. Andr. A semi-analytical model of the 3d boundary layer over the streamlined nose of a train. *Wind Engineering and Industrial Aerodynamics journal*, 119:78–88, 2013.

[17] D. E. Raveh. Computational-fluid-dynamics-based aeroelastic analysis and structural design optimizationa researchers perspective. *Computer Methods in Applied Mechanics and Engineering*, 194(40):3453–3471, 2005.

[18] D. M. Schuster, D. D. Liu, and L. J. Huttsell. Computational aeroelasticity: Success, progress, challenge. *AIAA Dynamics Specialists Conference*, 2003.

[19] C. Spada. Aeroelastic analysis of nonlinear high aspect ratio wings. Master's thesis, Instituto Superior Tcnico, October 2014.

[20] W. Stalewski and J. Sznajder. Application of a panel method with viscous-inviscid interaction for the determination od the aerodynamic characteristics of cesar baseline aircraft. *Transactions of the Institute of Aviation*, 207:63–83, 2013.